P_{IF}/P_{RF} for several LO powers. Since the power series (28) is valid only for a given range of the inputs, the macromodel is only valid within that range. The circles are simulation results using the time-domain simulator ASTAP [8], and show good agreement.

IV. Transfer Characteristics

The dashed lines in Fig. 2 demonstrate an important property of bivariate GPSA. Since the summation given by (19) contains powers of the phasor components as given by (14), any arbitrary input–ouptut transfer characteristic is of the form

$$Y_q = \sum_i H_{i,j}(X_j) \tag{29}$$

where $H_{i,j}$ is an ith-order nonlinear transfer function for the input phasor X_j (or set of X_j's). In general, $H_{i,j}$ is a function of the other input phasors. The dashed lines in Fig. 2 give (*a*) first-order, H_1, and (*b*) third-order, H_3, transfer characteristics for the IF phasor when $P_{LO} = 2.0$ dBm. In our example, the even-order transfer functions are zero. Note that in Fig. 2, the vertical axis is gain, not output amplitude; thus the lines represent the zeroth-order and second-order transfer characteristics for the gain, corresponding to the first- and third-order transfer characteristics for output amplitude. For the range modeled, all higher order transfer functions are negligible. Adding (*a*) and (*b*) yields a value within 1% of the total characteristic (solid line) shown for $P_{LO} = 2$ dBm. Thus a simple behavioral model is obtained by using only lower order powers of the input. Here, the nonlinear RF to IF characteristics can be described by the sum of two components. Each component can be represented as a linear function when expressed in log–log form.

V. Conclusion

The algebraic formula for the output of a nonlinearity described by a bivariate generalized power series having multifrequency inputs has been developed. These formulas enhance the capabilities of generalized power series analysis by allowing nonlinear functions of two variables to be considered in a general way. An example of a ring mixer has shown the practicality of this kind of analysis.

References

[1] S. L. Bussgang, L. Ehrman, and J. W. Graham, "Analysis of nonlinear systems with multiple inputs," *Proc. IEEE*, vol. 62, pp. 1088–1119, Aug. 1974.

[2] M. B. Steer and P. J. Khan, "An algebraic formula for the complex output of a system with multi-frequency excitation," *Proc. IEEE*, vol. 71, pp. 177–179, Jan. 1983.

[3] T. Narhi, "Multifrequency analysis of non-linear circuits using one and two dimensional series expansions," in *Proc. 19th European Microwave Conf.*, 1989.

[4] G. W. Rhyne, M. B. Steer, and B. D. Bates, "Frequency domain nonlinear circuit analysis using generalized power series," *IEEE Trans. Microwave Theory Tech.*, vol. 36, pp. 379–387, Feb. 1988.

[5] R. A. Nobakht, P. W. Pate, and S. H. Ardalan, "CAPSIM: A graphical simulation tool for communication systems," in *Proc. Globecom '88*, pp. 1692–1696.

[6] M. Abramowitz and I. A. Stegun, *Handbook of Mathematical Functions*. New York: Dover, 1965.

[7] B. W. Char, K. O. Geddes, G. H. Gonnet, and S. M. Watt, *Maple User's Guide*. Waterloo, Ont.: WATCOM Publications, 1985.

[8] W. T. Weeks *et al.*, "Algorithms for ASTAP—A network-analysis program," *IEEE Trans. Circuit Theory*, vol. CT-20, pp. 628–634, Nov. 1973.

Modeling of Asymmetric and Offset Gaps in Shielded Microstrips and Slotlines

ANIMESH BISWAS, MEMBER, IEEE, AND VIJAI K. TRIPATHI, SENIOR MEMBER, IEEE

***Abstract*—A generalized model for characterizing the frequency-dependent properties of general symmetric, asymmetric, and offset gaps in microstrips and slotlines on a single-layer or multilayer dielectric medium is presented. The transverse resonance technique is applied in the spectral domain to extract the equivalent circuit model parameters of the discontinuities. This technique incorporates the end effect of the discontinuity by a compatible choice of basis functions.**

I. Introduction

The characterization of symmetric and asymmetric gaps in microstrips and slotlines has been the subject of considerable interest in recent years since a knowledge of these discontinuity parameters is required for an accurate design of resonator elements and multiresonator filter circuits. The offset gaps in microstrips and slotlines provide an additional degree of freedom in terms of layout and design of coupled resonator filters. In addition, the analysis can also be helpful in estimating the coupling between offset coplanar conductors and slots in high-density microwave and millimeter-wave integrated circuits. A rigorous analysis for symmetric and asymmetric gaps in microstrips on suspended substrate has been presented by Koster and Jansen [1]. The accuracy of the method depends primarily on the choice of basis functions and can be verified by suitable experimental data. Experimental data for the end effect of open-ended slotline have been presented by Knorr [2]. This paper gives a general analysis of the gap discontinuities in both microstrip and slot structures, including offset gaps. The technique is based on an application of the transverse resonance technique proposed by Sorrentino and Itoh [3]. Here, the fields in various regions of the cavity are expanded in terms of hybrid modes whereas the slot fields and strip currents are expressed in terms of simple yet accurate basis functions. The validity of this type of basis function has been affirmed experimentally for the case of finline gap discontinuities [4].

II. Theory

The cross-sectional and longitudinal views of the general gap discontinuities in shielded microstrips and slotlines and their equivalent circuits are shown in Figs. 1 and 2. The electric and magnetic fields are expanded in terms of hybrid modes in each region and then the application of the boundary conditions at all the interfaces leads to the Green's dyadic as given in [4]. This is followed by the application of the Galerkin procedure in the transform domain, leading to a set of homogeneous equations as

Manuscript received October 10, 1989; revised December 15, 1989.

The authors are with the Department of Electrical and Computer Engineering, Oregon State University, Corvallis, OR 97331.

IEEE Log Number 9034894.

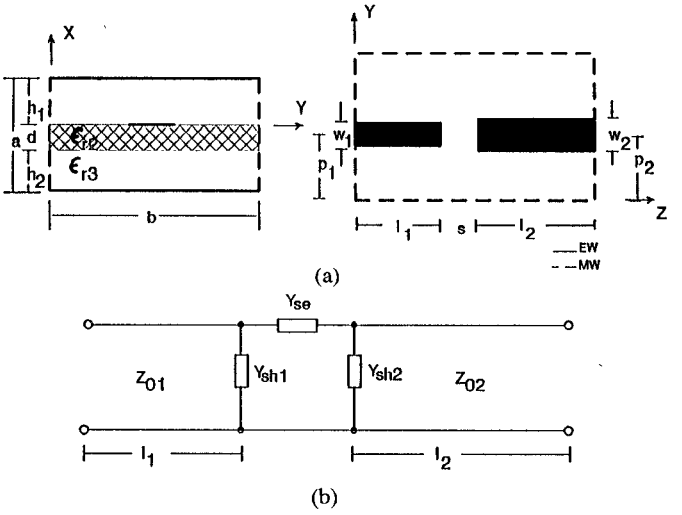

Fig. 1. (a) Cross-sectional and longitudinal views of suspended substrate cavity housing the discontinuity. (b) Equivalent circuit.

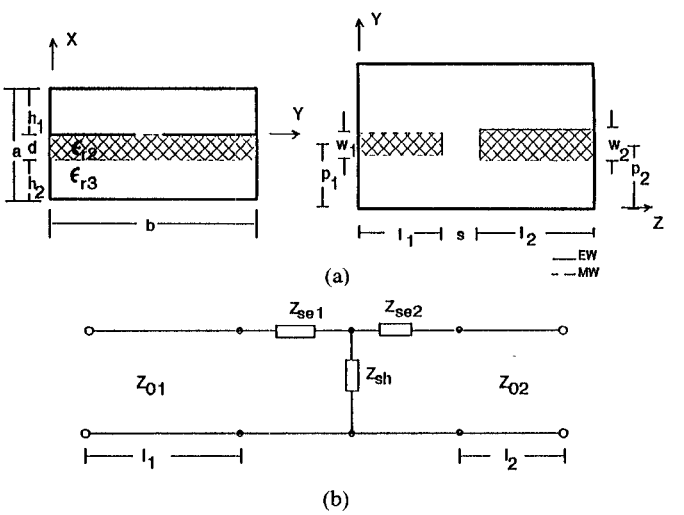

Fig. 2. (a) Cross-sectional and longitudinal views of shielded slotline cavity housing the discontinuity. (b) Equivalent circuit.

given by

$$\sum_{r=1}^{2}\sum_{p=1}^{\infty}\sum_{q=1}^{\infty} C_{pqr}\sum_{n=0}^{\infty}\sum_{m=1}^{\infty} P_nQ_mG_{11}L_{2mn}^{(p,q,r)}L_{2mn}^{(i,j,k)} + \sum_{r=1}^{2}\sum_{p=1}^{\infty}\sum_{q=1}^{\infty} D_{pqr}\sum_{n=0}^{\infty}\sum_{m=1}^{\infty} P_mQ_nG_{12}L_{1mn}^{(p,q,r)}L_{2mn}^{(i,j,k)} = 0$$

$$\sum_{r=1}^{2}\sum_{p=1}^{\infty}\sum_{q=1}^{\infty} C_{pqr}\sum_{n=1}^{\infty}\sum_{m=0}^{\infty} P_nQ_mG_{21}L_{2mn}^{(p,q,r)}L_{1mn}^{(i,j,k)} + \sum_{r=1}^{2}\sum_{p=1}^{\infty}\sum_{q=1}^{\infty} D_{pqr}\sum_{n=1}^{\infty}\sum_{m=0}^{\infty} P_mQ_nG_{22}L_{1mn}^{(p,q,r)}L_{1mn}^{(i,j,k)} = 0 \quad (1)$$

where

$$P_{n,m} = \begin{cases} 2, & n,m \neq 0 \\ 1, & n,m = 0 \end{cases}$$

$$Q_{n,m} = \begin{cases} 2, & n,m \neq 0 \\ 0, & n,m = 0 \end{cases}$$

$i = 1,2,\cdots,\infty$

$j = 1,2,\cdots,\infty$

$k = 1$ for odd mode

$k = 2$ for even mode.

Here, C_{pqr} and D_{pqr} are unknown coefficients of transformed fields (or currents) L_{2mn} and L_{1mn} at the aperture (or strip) plane. For the shielded microstrip case, the transformed currents can be written as

$$L_{2mn} = \int_0^b \int_0^{(l_1+l_2+s)} I_z(y,z)\cos(\alpha_n y)\sin(\beta_m z)\,dy\,dz$$

$$L_{1mn} = \int_0^b \int_0^{(l_1+l_2+s)} I_y(y,z)\sin(\alpha_n y)\cos(\beta_m z)\,dy\,dz. \quad (2a)$$

Similarly for the case of shielded slotline, the transformed fields are given by

$$L_{2mn} = \int_0^b \int_0^{(l_1+l_2+s)} E_y(y,z)\cos(\alpha_n y)\sin(\beta_m z)\,dy\,dz$$

$$L_{1mn} = \int_0^b \int_0^{(l_1+l_2+s)} E_z(y,z)\sin(\alpha_n y)\cos(\beta_m z)\,dy\,dz \quad (2b)$$

where

$$\alpha_n = \frac{n\pi}{b} \quad \text{and} \quad \beta_m = \frac{m\pi}{(l_1+l_2+s)}.$$

The elements of the Green function matrix in (1) for slotline and microstrip line are given by

$$G_{11}|_{\text{strip}} = \frac{\left\{\dfrac{\beta_m^2\Gamma_{mn1}}{j\omega\epsilon_0 F_{11}} - \dfrac{j\omega\mu_0\alpha_n^2}{F_{22}}\right\}\sin(\Gamma_{mn1}h_1)}{(\alpha_n^2+\beta_m^2)} \quad (3a)$$

$$G_{12}|_{\text{strip}} = G_{21}|_{\text{strip}} = \frac{\left\{\dfrac{\alpha_n\beta_m\Gamma_{mn1}}{j\omega\epsilon_0 F_{11}} + \dfrac{j\omega\mu_0\alpha_n\beta_m}{F_{22}}\right\}\sin(\Gamma_{mn1}h_1)}{(\alpha_n^2+\beta_m^2)} \quad (3b)$$

$$G_{22}|_{\text{strip}} = \frac{\left\{\dfrac{\alpha_n^2\Gamma_{mn1}}{j\omega\epsilon_0 F_{11}} - \dfrac{j\omega\mu_0\beta_m^2}{F_{22}}\right\}\sin(\Gamma_{mn1}h_1)}{(\alpha_n^2+\beta_m^2)} \quad (3c)$$

and

$$G_{11}|_{\text{slot}} = \frac{\left\{\dfrac{j\omega\epsilon_0\alpha_n^2}{\Gamma_{mn1}}\cdot F_{11} - \dfrac{\beta_m^2}{j\omega\mu_0}\cdot F_{22}\right\}}{(\alpha_n^2+\beta_m^2)\sin(\Gamma_{mn1}h_1)} \quad (4a)$$

$$G_{12}|_{\text{slot}} = G_{21}|_{\text{slot}} = \frac{\left\{\dfrac{j\omega\epsilon_0\alpha_n\beta_m}{\Gamma_{mn1}}\cdot F_{11} + \dfrac{\alpha_n\beta_m}{j\omega\mu_0}\cdot F_{22}\right\}}{(\alpha_n^2+\beta_m^2)\sin(\Gamma_{mn1}h_1)} \quad (4b)$$

$$G_{22}|_{\text{slot}} = \frac{\left\{\dfrac{j\omega\epsilon_0\beta_m^2}{\Gamma_{mn1}}\cdot F_{11} - \dfrac{\alpha_n^2}{j\omega\mu_0}\cdot F_{22}\right\}}{(\alpha_n^2+\beta_m^2)\sin(\Gamma_{mn1}h_1)} \quad (4c)$$

where

$$F_{11} = \cos(\Gamma_{mn1}h_1) - \epsilon_{r2}F_1\frac{\Gamma_{mn1}}{\Gamma_{mn2}}\sin(\Gamma_{mn1}h_1) \tag{5a}$$

$$F_{22} = \Gamma_{mn1}\cos(\Gamma_{mn1}h_1) + \Gamma_{mn2}F_2\sin(\Gamma_{mn1}h_1) \tag{5b}$$

$$F_1 = \frac{\{\epsilon_{r2}\Gamma_{mn3}\sin(\Gamma_{mn2}d)\sin(\Gamma_{mn3}h_2) - \epsilon_{r3}\Gamma_{mn2}\cos(\Gamma_{mn2}d)\cos(\Gamma_{mn3}h_2)\}}{\{\epsilon_{r2}\Gamma_{mn3}\cos(\Gamma_{mn2}d)\sin(\Gamma_{mn3}h_2) + \epsilon_{r3}\Gamma_{mn2}\sin(\Gamma_{mn2}d)\cos(\Gamma_{mn3}h_2)\}} \tag{5c}$$

$$F_2 = \frac{\{\Gamma_{mn3}\cos(\Gamma_{mn2}d)\cos(\Gamma_{mn3}h_2) - \Gamma_{mn2}\sin(\Gamma_{mn2}d)\sin(\Gamma_{mn3}h_2)\}}{\{\Gamma_{mn3}\sin(\Gamma_{mn2}d)\cos(\Gamma_{mn3}h_2) + \Gamma_{mn2}\cos(\Gamma_{mn2}d)\sin(\Gamma_{mn3}h_2)\}} \tag{5d}$$

$$\Gamma_{mn1} = \sqrt{\omega^2\mu_0\epsilon_0 - \alpha_n^2 - \beta_m^2} \tag{5e}$$

$$\Gamma_{mn2} = \sqrt{\omega^2\mu_0\epsilon_0\epsilon_{r2} - \alpha_n^2 - \beta_m^2} \tag{5f}$$

$$\Gamma_{mn3} = \sqrt{\omega^2\mu_0\epsilon_0\epsilon_{r3} - \alpha_n^2 - \beta_m^2}\,. \tag{5g}$$

In order to obtain the three unknown values of the equivalent circuit parameters shown in Figs. 1 and 2, we require three sets of solutions for l_1 and l_2. For a given frequency, and a fixed known values of l_1, length l_2 is computed from (1) by setting the determinant of the coefficient matrix equal to zero.

III. Field and Current Distributions

The basis functions for currents (or slot fields) are assumed to be symmetrical in the y direction since the variational nature of the Galerkin procedure is expected to lead to accurate results despite the asymmetric nature of these currents (or fields) for offset gaps. Here, the y and z components of the electric fields across the slots and currents in the strip are expressed as

$$I_z(y,z)\big|_{\substack{\text{odd}\\\text{even}}} = E_y(y,z)\big|_{\substack{\text{odd}\\\text{even}}} = f_{11}(y)f_1(z) \mp f_{12}(y)f_2(z)$$

$$I_y(y,z)\big|_{\substack{\text{odd}\\\text{even}}} = E_z(y,z)\big|_{\substack{\text{odd}\\\text{even}}} = f_{21}(y)f_3(z) \mp f_{22}(y)f_4(z) \tag{6}$$

where

$$f_{1i}(y) = \left[(w_i/2)^2 - (y-p_i)^2\right]^{-1/2}, \qquad |(y-p_i)| \leqslant w_i/2$$

$$f_{2i}(y) = (y-p_i)\left[(w_i/2)^2 - (y-p_i)^2\right]^{1/2}, \quad |(y-p_i)| \leqslant w_i/2$$

$$i = 1,2 \tag{7a}$$

$$\begin{bmatrix} f_1(z) \\ f_3(z) \end{bmatrix} = \begin{matrix} \sin \\ \cos \end{matrix}\left[\frac{2\pi z}{\lambda_1}\right], \qquad 0 < z < \lambda_1/4$$

$$= \begin{matrix} \sin \\ -\cos \end{matrix}\left[\frac{\pi(l_1 - z)}{(2l_1 - \lambda_1/2)}\right], \qquad \lambda_1/4 < z \leqslant l_1 \tag{7b}$$

$$\begin{bmatrix} f_2(z) \\ f_4(z) \end{bmatrix} = \begin{matrix} \sin \\ \cos \end{matrix}\left[\frac{\pi(z - l_1 - s)}{(2l_2 - \lambda_2/2)}\right],$$

$$(l_1 + s) < z \leqslant (l_1 + l_2 + s - \lambda_2/4)$$

$$= \begin{matrix} \sin \\ \cos \end{matrix}\left[\frac{2\pi}{\lambda_2}(z - l_1 - l_2 - s + \lambda_2/2)\right],$$

$$(l_1 + l_2 + s - \lambda_2/4) < z \leqslant (l_1 + l_2 + s) \tag{7c}$$

where λ_1 and λ_2 are the dominant mode wavelengths of uniform slot or microstrip lines of widths w_1 and w_2, respectively, and p_1 and p_2 are offset parameters of strip or slot. At the time of computation, length l_1 is chosen to have a value close to $\lambda_1/2$. Equations (7b) and (7c) are illustrated in Fig. 3 to show the effect of end correction for open-end strip or slotline.

IV. Results

The computation of the resonant length of the cavity in the presence of the gap discontinuity was carried out by truncating the series in (1) to 200 terms. Generally, the number of terms chosen in (1) depends on the operating frequency and the dimensions of the housing. It is seen that for the results presented in this paper, 200 terms lead to an evaluation of the resonant length of the cavity accurate to within about 1%. In order to validate the z variation of our basis functions, the computed results based on the technique presented here are compared with published experimental data [2] for slotline end effect in Fig. 4. The agreement is seen to be fairly good. Fig. 5 shows the variations in the equivalent circuit parameters for an asymmetric gap for the case of microstrip on suspended substrate. These results are slightly different from those given in [1], which could be due to the choice of basis functions. Fig. 6 shows the variation in the equivalent circuit parameters as a function of the width ratio of the asymmetric gap in the slotline case. The series capacitance for the microstrip case and the shunt inductance for the slotline case increase with an increase in the strip and slot width ratio respectively and, as expected, acquire an asymptotic value for large ratio. Figs. 7 and 8 show the variation of equivalent circuit parameters of the offset gap discontinuity in microstrip and slotline respectively. It can be seen from these figures that the series capacitance for the microstrip case and the shunt inductance for the slotline case decrease almost exponentially as p_2/p_1 decreases. This behavior is expected since the interactions between the lines decrease with a decrease in the p_2/p_1 ratio. For the limiting case, the discontinuity behaves as an open circuit for the microstrip case and a short circuit for the slotline case.

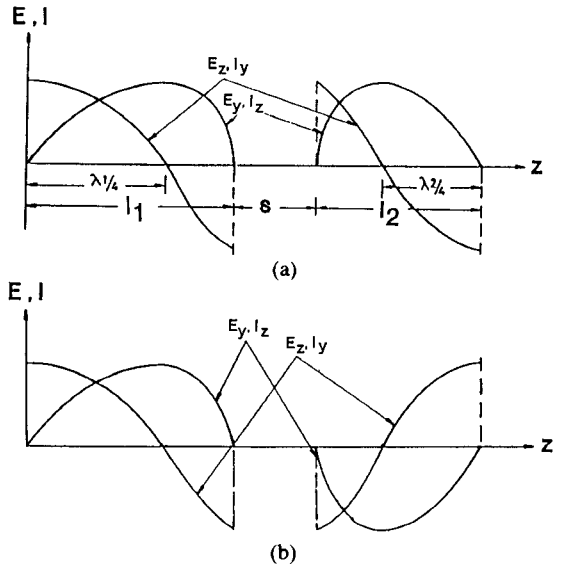

Fig. 3. z variation of strip current and slot field: (a) even-mode excitation; (b) odd-mode excitation.

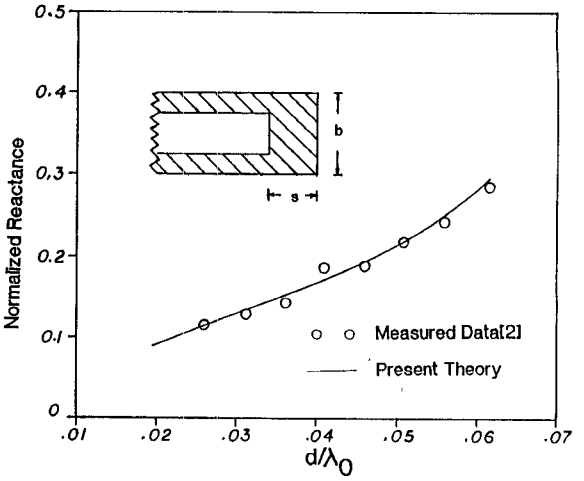

Fig. 4. Comparison of theoretical and experimental data [2] for short-circuit reactance of a slotline. $\epsilon_{r2} = 12.0$, $\epsilon_{r3} = 1.0$, $b = 46.78$ mm, $h_1 = 15.367$ mm, $h_2 = 15.367$ mm, $d = 3.0734$ mm, $w/d = 0.221$, $s = 9.23$ mm.

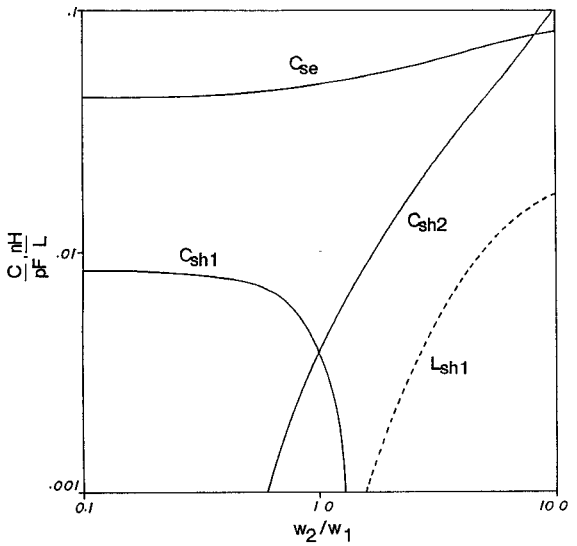

Fig. 5. Variation of reactance parameters of asymmetric gap in microstrip on a suspended substrate with strip width ratio: $a = 40$ mm, $b = 40$ mm, $h_2 = d = 0.635$ mm, $w_1 = 0.635$ mm, $s = 0.09525$ mm, $\epsilon_{r2} = 10.4$, $\epsilon_{r3} = 1.0$, frequency = 4.0 GHz, $p_1 = p_2 = 20$ mm.

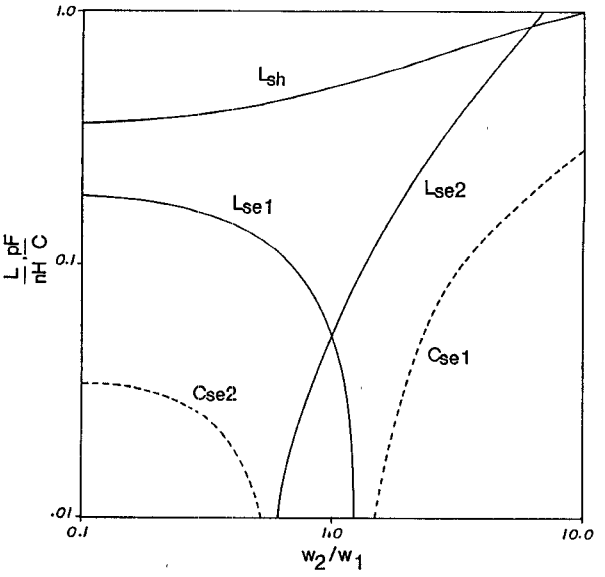

Fig. 6. Variation of reactance parameters of asymmetric gap in slotline with slot width ratio: $a = 40$ mm, $b = 40$ mm, $h_1 = 20$ mm, $d = 0.635$ mm, $\epsilon_{r2} = 9.8$, $\epsilon_{r3} = 1.0$, $w_1 = 0.635$ mm, $s = 0.2$ mm, $p_1 = p_2 = 20$ mm, frequency = 4.0 GHz.

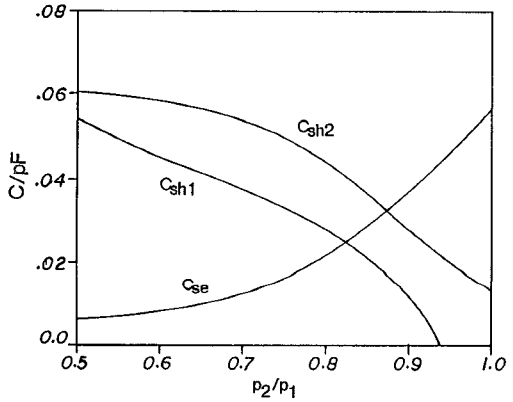

Fig. 7. Variation of reactance parameters of asymmetric gap in microstrip on a suspended substrate with strip offset parameters: $a = 40$ mm, $b = 40$ mm, $\epsilon_{r2} = 10.4$, $\epsilon_{r3} = 1.0$, $h_2 = d = 0.635$ mm, $w_1 = 0.635$ mm, $w_2 = 1.27$ mm, $s = 0.09525$ mm, $p_1 = 20$ mm, frequency = 4.0 GHz.

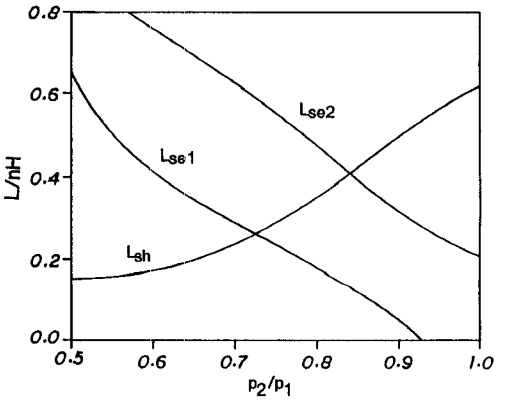

Fig. 8. Variation of reactance parameters of asymmetric gap in slotline with slot offset parameters: $a = 40$ mm, $b = 40$ mm, $\epsilon_{r2} = 9.8$, $\epsilon_{r3} = 1.0$, $h_1 = 20$ mm, $d = 0.635$ mm, $w_1 = 0.635$ mm, $w_2 = 1.27$ mm, $s = 0.2$ mm, $p_1 = 20$ mm, frequency = 4.0 GHz.

V. Conclusion

A numerical method used to solve for the frequency-dependent characteristics of symmetric, asymmetric, and offset inductive and capacitive gaps in shielded slotline and microstrip lines has been presented. With a simple yet accurate basis function, this technique leads to an accurate evaluation of the equivalent circuit parameters of these discontinuities.

References

[1] N. Koster and R. Jansen, "The equivalent circuit of the asymmetrical series gap in microstrip and suspended substrate line," *IEEE Trans. Microwave Theory Tech.*, vol MTT-30, Aug. 1982.

[2] J. B. Knorr and J. Saenz, "End effect in a shorted slot," *IEEE Trans. Microwave Theory Tech.*, vol. MTT-21, pp. 579–580. Sept. 1973.

[3] R. Sorrentino and T. Itoh, "Transverse resonance analysis of finline discontinuity," *IEEE Trans. Microwave Theory Tech.*, vol. MTT-30, Dec. 1984.

[4] A. Biswas and B. Bhat, "Accurate characterization of an inductive strip in finline," *IEEE Trans. Microwave Theory Tech.*, vol. 36, Aug. 1988.

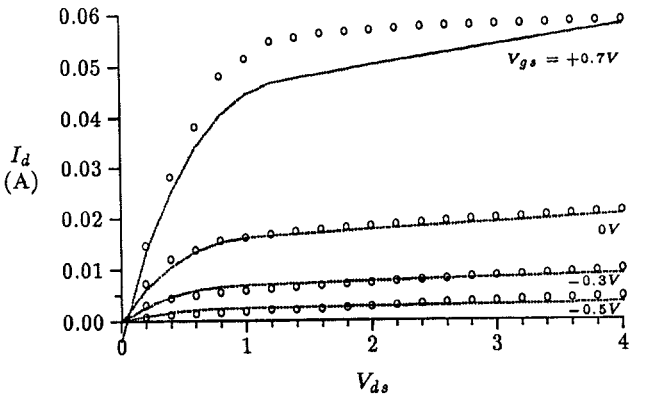

Fig. 1. As illustrated for a 0.6 V pinch-off GaAs MESFET, the Statz model (solid lines) shows poor tracking of the drain–source resistance as the gate bias is varied. The model parameters were chosen to fit measured data (∘) at an intermediate gate bias.

An Improved GaAs MESFET Model for SPICE

ANGUS J. McCAMANT, GARY D. McCORMACK, AND DAVID H. SMITH

Abstract—**A SPICE model has been developed to more accurately model GaAs MESFET devices. In particular, small-signal parameters such as the S parameters are accurately modeled over a wide range of bias conditions. These results were achieved by modifying the Statz [1] model equations to better represent the variation of I_{ds} as a function of the applied voltage.**

The model applies over a large range of pinch-off voltages, allows size scaling of devices, and is suited for modeling R_{ds} changes with frequency. The Statz equations are used to represent diode characteristics and capacitive components of the model.

I. Introduction

Since the commercial development of GaAs MESFET IC technology, the past decade has seen a proliferation of proposed models for GaAs MESFET's. Of these, the most frequently cited and most widely used are the models proposed by Curtice [2] and an improved model put forward by Statz *et al.* [1]. The Curtice model is derived from the Shichmann–Hodges JFET model [3] modified to provide a proper knee voltage for the I–V curves. The Statz model additionally provides an improved representation of the capacitance behavior.

The purpose of the current work is to model specific features of MESFET behavior which neither the Curtice nor the Statz equations properly describe. It is shown that the resulting model equations provide an improved fit to measured MESFET characteristics without increased complexity.

II. Deficiencies of Existing Models

A typical result obtained when attempting to fit the Statz model to measured I–V data is illustrated in Fig. 1. Notice particularly the slope of the I–V curves, the drain conductance.

Manuscript received November 6, 1989; revised February 26, 1990.
The authors are with TriQuint Semiconductor, Inc., Beaverton, OR 97076.
IEEE Log Number 9035406.

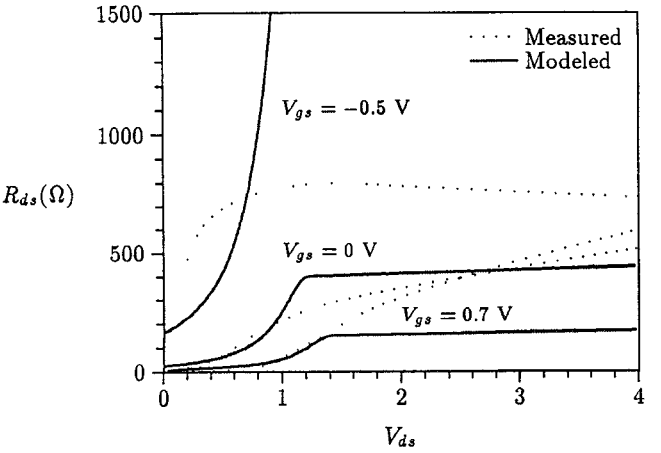

Fig. 2. The Statz model does not track measured drain resistance, R_{ds}, well as the gate bias is varied. The measured data are extracted from S-parameter data. As illustrated in the figure, the tracking is especially poor when V_{gs} is near cutoff. The sharp change in slope near 1.2 V is a result of using the cubic polynomial approximation in the Statz equations.

As with most proposed GaAs MESFET models, the drain conductance is modeled by multiplying the expression for I_{ds} by a term: $(1+\lambda V_{ds})$. While this term can represent drain conductance at a particular bias point, it does not model variations with bias correctly, predicting a conductance which increases at higher values of I_{ds}, while the observed conductance actually decreases.

The Statz model also fails to provide an accurate model at low currents where V_{gs} is near cutoff. In particular, the drain conductance derived from the Statz equation, illustrated in Fig. 2, does not fit well.

The differences between the measured and modeled dc I–V curves are reflected in erroneous predictions of small-signal parameters such as gain and drain resistance over the dynamic range of the device. The improper tracking of these parameters with bias leads to incorrect predictions of such performance characteristics as gain compression and harmonic distortion.

Proposed models that fit drain conductance variations better than the Statz model include that by Materka [4] and the Curtice cubic [5], but these models suffer from other disadvan-